Spin tunneling in multilayer spintronic devices

S. G. Tan,[1] M. B. A. Jalil,[2] S. Bala Kumar,[1,2] and G.-C. Liang[3]
[1]*Data Storage Institute, DSI Building, 5 Engineering Drive 1 (Off Kent Ridge Crescent, National University of Singapore), Singapore 117608, Singapore*
[2]*Information Storage Materials Laboratory, Electrical and Computer Engineering Department, National University of Singapore, 4 Engineering Drive 3, Singapore 117576, Singapore*
[3]*Silicon Nano Device Laboratory, Electrical and Computer Engineering Department, National University of Singapore, 4 Engineering Drive 3, Singapore 117576, Singapore*
(Received 23 July 2007; published 20 February 2008)

We introduce a spin tunneling theory across the interfaces of multilayer spintronic devices, e.g., spin valves and magnetic random access memories, which integrates the microscopic Green's function formalism for electron propagation within the interfacial barrier with the macroscale spin-dependent Boltzmann theory, which governs the spin accumulation in the adjacent contacts. This multiscale approach makes possible the detailed studies of interfacial properties (e.g., height, shape, and spin asymmetry) required to achieve high spin injection via tunneling. Based on the calculated results, the optimal interfacial properties have been identified for possible experimental verification.

DOI: 10.1103/PhysRevB.77.085424 PACS number(s): 72.25.Hg, 73.40.Gk, 85.75.−d

I. INTRODUCTION

Electron propagation through potential barriers, which are induced either by interfacial roughness between adjacent layers, systematic doping of bulk layers with impurities, band alignment between different layer materials, or external potential applied locally, plays a crucial role in multilayer devices, e.g., spin valve sensors,[1–5] magnetic tunnel junctions,[6,7] lateral spintronic devices,[8–11] and traditional complementary metal oxide semiconductor transistors. In fact, in semiconductor spintronic devices, the presence of tunneling barriers can greatly enhance spin injection efficiency from a ferromagnetic metal electrode into the semiconductor device.[12–14] Even in conventional ferromagnetic metal multilayers, spin-dependent scattering at the layer interfaces, as opposed to scattering in the bulk, provides a significant contribution to the giant magnetoresistance (MR) effect.[15–17] Conversely, spin flip at the interfaces can result in a large suppression of MR.[18] More recently, basic understanding of the ballistic tunneling process through barriers[19] and rapid advances in nanofabrication techniques have improved the capability of engineering interfacial barriers with significantly better performance.[20]

In this paper, we develop a multiscale spin transport theory for the investigation of tunneling spin injection, which is an important phenomenon for spintronic applications. Spin current due to conduction electrons is a nonconserved quantity and, thus, the efficiency with which it is transmitted from a magnetic source layer to a usually nonmagnetic collector layer is crucially determined by the physics of the electron propagation and transmission through the interfacial barrier. Therefore, the spin injection process warrants a detailed analysis beyond the conventional macroscopic picture. Previous theoretical investigations of spin injection across a tunnel barrier are either based on the purely semiclassical spin drift-diffusive approach[12,21] (which treats the barrier as a lump resistance element) or by focusing on the ballistic tunneling across the barrier region.[22,23] In our work, we apply the effective mass Green's function formalism[24–28] to analyze the microscopic effects of the tunnel barrier potential on the incident spin current. At the same time, the transmitted spin current is also dependent on the spin accumulation and resulting electrochemical potential at the two adjacent contacts. The spin accumulation on the contacts can be determined by considering the semiclassical spin-dependent drift-diffusive transport (based on the Boltzmann equation) within the bulk of the contacts.[12,29–32] Thus, the main focus of this paper is to (1) introduce a self-consistent approach that combines the microscopic Green's function formalism within the nanoscale barrier and the Boltzmann drift-diffusive model within the macroscopic contacts and, (2) based on this model, study the effects of barrier properties, e.g., potential profile and geometry, on the tunneling transport in order to optimize the tunneling spin injection for potential spintronic applications.

The basic structure under consideration (shown in Fig. 1) is a multilayer device comprising a bulk ferromagnetic (FM) left layer acting as the spin injector, a thin interface (I), and the bulk semiconductor (SC) right layer, which receives the injected spin current. The interfacial barrier is located within the semiconductor region. At equilibrium, the Fermi levels of the SC and FM layers are equalized, but under an applied electrical bias, a nonequilibrium electrochemical profile is obtained, typically as shown in Fig. 1 (top). Note that in both the FM and SC layers, there will be a split in the spin-up and spin-down electrochemical potentials in the vicinity of the interfacial barrier, resulting in spin accumulation. In most previous works utilizing Green's function analysis, the electrochemical potentials adjacent to the barrier on both sides are treated as a reservoir constant, i.e., independent of the nature of electron propagation within the barrier. In the bulk spin drift-diffusion approach, electron transport in the magnetic multilayers has been modeled based on purely passive factors, such as device geometry, resistivity, and the different spin diffusion lengths in its constituent layers. In our self-consistent, multiscale approach, however, the spin-dependent electrochemical potentials and the tunneling resistance

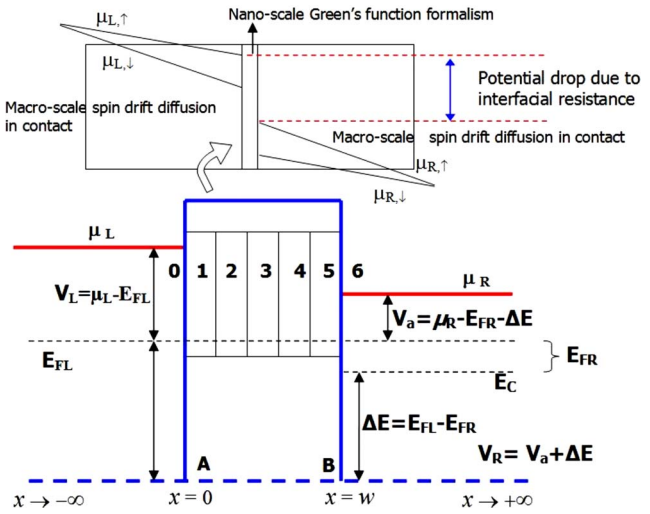

FIG. 1. (Color online) (Top) Nonequilibrium distribution of electrochemical potential across the multilayer structure under electrical bias. (Bottom) Magnified diagram of the interfacial barrier of thickness $w=2.5$ nm, which is spatially discretized into $n=5$ planar sections for the Green's function analysis. $\mu_{L\uparrow}$ ($\mu_{R\uparrow}$) indicates the spin-up electrochemical potential at the boundaries of the barrier, i.e., at A and B. E_{FL} (E_{FR}) is the equilibrium Fermi level of the left (right) contacts. E_C indicates the conductance band of the semiconductor. For clarity, only the spin-up potentials are drawn.

across the barrier are solved self-consistently by combining the microscopic Green's function model within the barrier and the drift-diffusive model in the contacts, as illustrated schematically in Fig. 2. The calculation begins by assuming initial values of the charge current density ($\mathbf{j_p}=\mathbf{j_{p\uparrow}}+\mathbf{j_{p\downarrow}}$) and interface resistance ($\mathbf{R_I}$). Based on the spin-dependent drift-diffusion equations, the spatial distribution of the electrochemical profile within both the FM and SC leads can be determined. Subsequently, the evaluated electrochemical potential values at sites immediately adjacent to the barrier are input as variables in the Green's function calculation of electron transmission through the barrier. The microscopic model within the barrier constitutes a parallel scheme to determine the current density ($\mathbf{j_g}$) and the interfacial resistance ($\mathbf{R_F}$). The calculation cycle is repeated until the current densities $\mathbf{j_p}$ and $\mathbf{j_g}$, and hence the corresponding interfacial resistances $\mathbf{R_I}$ and $\mathbf{R_F}$, converge. In this way, we will have unified the microscopic Green's function and macroscopic drift-diffusion

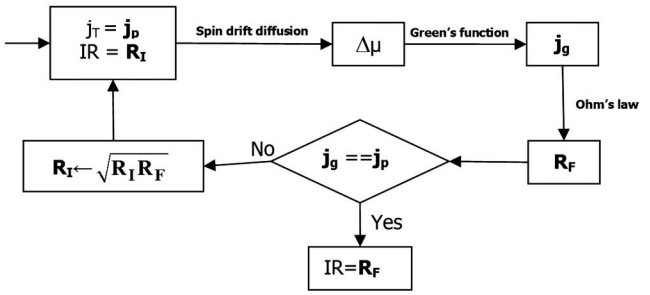

FIG. 2. Self-consistent calculation scheme for interfacial resistance and current density, which is iterated until the current density converges.

models within and outside the barrier, respectively, and obtained the effective tunneling resistance value which is consistent with both models.

Thus, the nonequilibrium potentials at the leads are coupled to the Green's function calculation for transport within the barrier. One consequence of this self-consistent approach is that the effective barrier resistance as seen by the spin-up and spin-down electrons becomes a dynamical quantity which depends on external factors such as the applied bias, instead of a static parameter which is solely dependent on the intrinsic barrier properties. The resulting spin injection efficiency in the multilayer will be a function of external parameters, e.g., the applied voltage bias or current density,[33,34] in agreement with recent experimental observations. Thus, our model can incorporate spin transport effects that may have been neglected by previous models. The analysis of these effects, such as the increase in spin asymmetry of tunneling conductance with increasing barrier height and barrier potential spin asymmetry, may potentially guide experimental efforts to engineer interfacial barriers for optimal spin injection.

II. THEORY

A. Green's function formalism

The interfacial (I) central region of the three-region device of Fig. 1, of thickness $w=2.5$ nm, is discretized into n planar sections. The number of discrete sections is chosen to be $n=5$ such that the width of each section $a=(w/n)=0.5$ nm is smaller than the Fermi wave vector $\lambda_F \approx 1.5$ nm, thus ensuring accuracy of the tight-binding Green's function calculations. The left FM and the right SC regions are both treated as semi-infinite in width. Following the tight-binding lattice formalism, the matrix representation of the Schrödinger equation can be expressed as

$$\begin{bmatrix} E+i\eta-H_L & \tau^{LC} & 0 \\ \tau^{CL} & E-H_C & \tau^{CR} \\ 0 & \tau^{RC} & E+i\eta-H_R \end{bmatrix} \begin{bmatrix} G^L & G^{LC} & 0 \\ G^{CL} & G^C & G^{CR} \\ 0 & G^{RC} & G^R \end{bmatrix} = I, \tag{1}$$

where $E+i\eta-H_{L,R}$ is an $M\times M$ infinite matrix that describes the left (right) contact from site 0 (6) onward to the left (right), τ^{LC} (τ^{RC}) is the coupling matrix between the left (right) contacts to the central region and has dimensions of $M\times 5$, and τ^{CL} (τ^{CR}) is the transpose of the coupling matrix of dimensions of $5\times M$, i.e., $\tau^{CL}=(\tau^{LC})^T$ and $\tau^{CR}=(\tau^{RC})^T$. The central region is described by $E-H_C$, a 5×5 matrix representing the discrete sites 1–5 of the central region. Matrix multiplication results in

$$(E+i\eta-H_L)G^{LC}+\tau^{LC}G^C=0,$$

$$(E+i\eta-H_R)G^{RC}+\tau^{RC}G^C=0. \tag{2}$$

The above equations can be expressed as $G^{LC}=-\tilde{g}^L\tau^{LC}G^C$ and $G^{RC}=-\tilde{g}^R\tau^{RC}G^C$, where G^{LC} and G^{RC} are semi-infinite $M\times 5$, and $\tilde{g}^L$ and $\tilde{g}^R$ are the $M\times M$ Green's function

matrices of $(E+i\eta-H_L)^{-1}$ and $(E+i\eta-H_R)^{-1}$ for the isolated left and right contacts, respectively. From Eq. (1), we also obtained the matrix equation $(E-H_C)G^C+\tau^{CL}G^{LC}+\tau^{CR}G^{RC}=I$. Substituting the above expressions for G^{LC} and G^{RC}, we obtained $(E-H_C-\tau^{CL}\tilde{g}^L\tau^{LC}-\tau^{CR}\tilde{g}^R\tau^{RC})G_C=I$. Thus, the Green's function matrix for the central region can be expressed by $G_C=(E-H_C-\Sigma^L-\Sigma^R)^{-1}$, where Σ^L and Σ^R are the 5×5 self-energy matrices due to adjacent sites on the contacts to the left and right of the central region. The explicit form of G^C is given by

$$G^C=\begin{bmatrix} E-H_{C1}-t_Lg_0t_L & t & 0 & 0 & 0 \\ t & E-H_{C2} & t & 0 & 0 \\ 0 & t & E-H_{C3} & t & 0 \\ 0 & 0 & t & E-H_{C4} & t \\ 0 & 0 & 0 & t & E-H_{C5}-t_Rg_6t_R \end{bmatrix}^{-1}, \tag{3}$$

where $H_{Cj}=(2t+U_j)$ for $j=1,\ldots,5$, with U_j being the localized potential at the lattice site j, $t=\hbar^2/2ma^2$, i.e., the energy coupling constant between adjacent discrete sites, and a is the distance between them. The Green's function g_0 (g_6) is for site 0 (6) on the left (right) contact, and they are respectively the components of matrices $\tilde{g}^L(\tilde{g}^R)$. Before the inverse matrix of Eq. (3) can be evaluated, we require the explicit expression for the self-energies of $t_Lg_0t_L$ and $t_Rg_6t_R$, where t_L and t_R are matrix components of τ^L and τ^R, respectively. These may be, (1) in the simplest case, assigned empirical constant values[35], (2) numerically calculated by renormalization method,[28,36] or (3) analytically derived from the surface Green's function of a semi-infinite lead. In the one-dimensional single mode form, as an approximation, the flat-potential analytic Green's function for the semi-infinite left and right leads is given by $g_{06}=-(1/t)\exp(ik_{L,R}a)$, where $k_{L,R}=\sqrt{2m(E-V_{L,R})}/\hbar=\sqrt{2m(E-\mu_{L,R}+E_{FL,R})}/\hbar$, with $E_{FL,R}$ the equilibrium Fermi level of the left and right contacts, $\mu_{L,R}$ the nonequilibrium electrochemical potential incident on the left and right side of the barrier, and V_R the energy quantity as described in Fig. 1. To calculate the current perpendicular to the multilayer plane at a particular site, we consider the ballistic spin current expression of Eq. (4), which could be developed from Caroli *et al.*,[24]

$$J_0^\sigma=\sum_{k_{//}}\frac{-e}{A\hbar}\int\frac{dE}{2\pi}(f_L^\sigma-f_R^\sigma)(\Gamma_{11}^\sigma G_{15}^{r\sigma}\Gamma_{55}^\sigma G_{51}^{a\sigma}), \tag{4}$$

where $\Gamma_{11}=it_{10}^2(g_0^r-g_0^a)$, $\Gamma_{55}=it_{56}^2(g_6^r-g_6^a)$ (with subscripts r and a referring to the retarded and advanced Green's functions, respectively), A is the device cross sectional area, σ is the index for spin up and spin down, and $f_{L,R}^\sigma=1/[1+\exp(E-\mu_{L,R}^\sigma)/kT]$ is the Fermi occupation probability. Since the nonequilibrium Green's function applies only to the interfacial potential in the SC region and assuming that the SC material has a uniform effective mass over the transverse x-y plane, $T(E)=(\Gamma_{11}^\sigma G_{15}^{r\sigma}\Gamma_{55}^\sigma G_{51}^{a\sigma})$ will be independent of $k_\parallel$. Thus, current can be calculated as

$$J_0^\sigma=\frac{-e}{\hbar}\int\frac{dk_{//}}{4\pi^2}\int\frac{dE}{2\pi}(f_L^\sigma-f_R^\sigma)T(E). \tag{5}$$

The final current expression is

$$J_0^\sigma=\frac{-2\pi mekT}{h^3}\int_{-\infty}^{+\infty}dET(E)(F_L^\sigma-F_R^\sigma), \tag{6}$$

where $F_{L,R}^\sigma=\ln[1+\exp(\mu_{L,R}^\sigma-E)/kT]$.

B. Boltzmann drift-diffusive model

The Green's function calculations described in the previous section require the electrochemical potential values of μ_0, $\mu_\uparrow$, and $\mu_\downarrow$ at the left (right) boundaries between the central region and the semi-infinite FM (SC) contacts. These have to be determined by evaluating the electrochemical potential profile within the bulk FM and SC leads using the macroscopic spin drift-diffusion theory based on the Boltzmann equation. In this model, the spin accumulation $\Delta\mu_i(x)=\mu_i^\uparrow(x)-\mu_i^\downarrow(x)$ ($i=L,R$ is the lead index) assumes the following spatial distribution:

$$\Delta\mu_i(x)=A_i\exp\left(\frac{x}{\lambda_i}\right)+B_i\exp\left(-\frac{x}{\lambda_i}\right), \tag{7}$$

which is the solution to the spin diffusion equation $\partial^2\Delta\mu/\partial x^2=\Delta\mu/\lambda^2$, with λ being the spin relaxation length. Although $\Delta\mu$ is a steady-state value, it is sustained by the spin-polarized currents (i.e.. $j_\uparrow$ and $j_\downarrow$) in the system. When these currents are removed, $\Delta\mu$ will decay to zero due to spin relaxation. Additionally, the individual potentials $\mu_{\uparrow,\downarrow}$ also obey the drift equation given by $j_{\uparrow(\downarrow)}=-\sigma_{\uparrow(\downarrow)}(\partial\mu_{\uparrow(\downarrow)}/\partial x)$, where the subscripts $\uparrow$ and $\downarrow$ refer to the up and down spin orientations, and $\sigma_{\uparrow(\downarrow)}=(1\pm\alpha)\sigma_0/2$ is the spin-dependent conductivity (with α being the material's intrinsic spin polarization of conductivity and σ_0 its spin-independent conductivity). The coefficients A_i and B_i in Eq. (7) are obtained by applying the appropriate boundary conditions,[16] e.g., spin current continuity and potential discontinuity due to the interfacial barrier resistance. The poten-

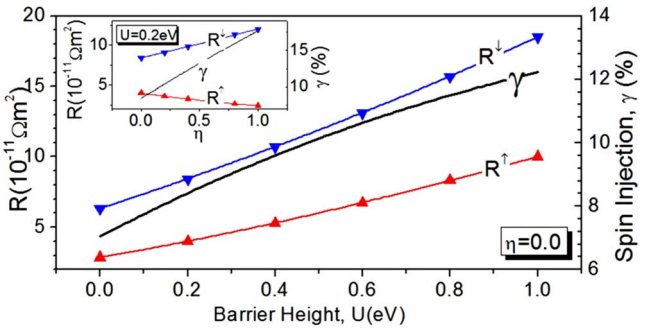

FIG. 3. (Color online) Left axis: Spin-up and spin-down resistances as a function of interfacial barrier height U. The difference of resistances becomes increasingly more divergent with U. Right axis: Tunneling spin injection ratio γ increases with U due to the increasingly spin-asymmetric resistances. Inset: Spin-up and spin-down resistances (left axis) and spin injection ratio (right axis) as a function of spin asymmetry η of barrier potential, with $U_\uparrow$ fixed at 0.2 eV.

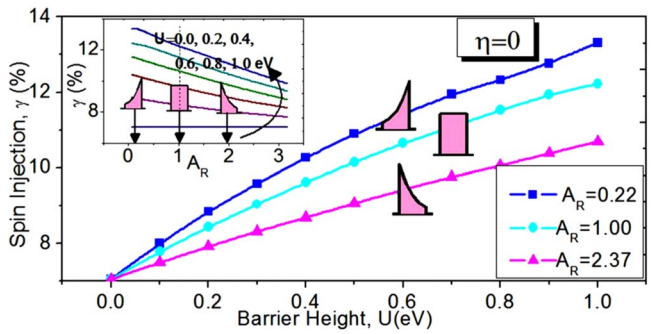

FIG. 4. (Color online) Spin injection ratio γ as a function of barrier height U and barrier geometry as characterized by A_R. The barriers considered have zero spin asymmetry (η=0) and the same area under their respective potential curve.

tial discontinuity at the interface due to the interfacial resistance is described by the following equation: $-eJ_0^\sigma R_I^\sigma = \mu_R^\sigma - \mu_L^\sigma$, where R_I^σ is the areal spin-dependent interfacial resistance experienced by electrons at the interface. The electrochemical potential $\mu_{R,L}^\sigma$ at the interfaces and R_I^σ are solved self-consistently by combining the microscopic Green's function model within the barrier and the Boltzmann drift-diffusive model in the contacts, as illustrated schematically in Fig. 2. Having solved Eq. (7), we have thus determined the electrochemical potential values at the contact-central region boundaries. These are then input into the next iteration of Green's function calculations, thus completing the self-consistent calculation cycle.

III. RESULTS AND DISCUSSION

Based on the above self-consistent scheme, we calculate the resistances $R_\uparrow$ and $R_\downarrow$ as experienced by the spin-up and spin-down electrons, respectively, and the spin injection ratio, defined as $\gamma=(j_\uparrow - j_\downarrow)/(j_\uparrow + j_\downarrow)$ at $x=w$. Unless otherwise stated, we assume the following parameter values in our calculations:[37–40] $j=10^6$ A/cm^2, resistivity $(\rho_{\mathrm{FM}}, \rho_{\mathrm{SC}}) = (10^{-7}, 10^{-4})$ Ω m, intrinsic spin polarization ratio $(\alpha_{\mathrm{FM}}, \alpha_{\mathrm{SC}}) = (0.4, 0.0)$, effective mass $(m^*_{\mathrm{FM}}, m^*_{\mathrm{SC}}) = (1, 0.067) m_e$, and Fermi energy $(E_{F.\mathrm{FM}}, E_{F,\mathrm{SC}}) = (10, 0.05)$ eV. Figure 3 shows that both the magnitude $(R_\uparrow + R_\downarrow)$ and spin asymmetry $(R_\uparrow - R_\downarrow)$ of the interfacial barrier resistance increase with interfacial barrier height U, even when the barrier height is spin independent (i.e., η=0). While the former is a well-established fact, the latter is a rather unexpected result arising out of the self-consistent, multiscale calculations. This is because the semiclassical spin drift-diffusive models predict high spin injection only in the presence of spin-asymmetric tunnel barriers.[12] The divergence between the $R_\uparrow$ and $R_\downarrow$ with increasing barrier height naturally leads to a higher spin injection ratio, as by the γ curve of Fig. 3. Additionally, as shown in the inset of Fig. 3, the divergence between the spin-up and spin-down resistances also increases with increasing spin asymmetry $\eta = (U_\downarrow - U_\uparrow)/(U_\uparrow + U_\downarrow)$ of the barrier potential, thus enhancing the spin injection ratio through the barrier. It is worth noting that the increase of spin injection ratio with increasingly divergent spin resistance is consistent with previous theoretical results.[12] Since it has been previously predicted that spin injection efficiency may be improved by increasing the spin asymmetry of the tunneling barrier potential, considerable experimental efforts have been focused on engineering suitable tunneling barrier with a large spin-split property. Our calculations, however, suggest that high spin injection efficiency may also be achieved by engineering a suitably high barrier potential, without necessarily having to enhance its spin-split property, which is a more challenging proposition in practical tunnel barriers. Thus, the fact that the spin asymmetry of barrier resistance is sensitive to the barrier height is a useful result of our work. Further, it is instructive to conduct a systematic study of how the divergence between the spin-up and spin-down resistances is influenced by specific tunnel barrier profiles and thickness.

We consider three types of barrier potentials: (1) exponentially increasing (in going from the FM to the SC layer), (2) exponentially decreasing, and (3) square profiles. These barrier profiles are visually depicted in the inset of Fig. 4. For a quantitative description of the barrier profile, we introduce a variable $A_R=(U_0/U)$, which is the ratio of the barrier potential at $x=0$ (U_0) to the height of an equivalent square barrier (U). Barriers of the same thickness w can be considered equivalent when the area under their respective barrier potentials are equal. This is because for barriers with identical w, the area under the barrier represents the average potential experienced by the tunneling electron while traversing across the barrier. By keeping the area under the barrier constant, we thus have $A_R<1$ $(A_R>1)$ for the exponentially increasing (decreasing) potentials and $A_R=1$ for the square barrier. We first consider the effect of barrier height for three representative barrier potentials with specific A_R values of 0.22, 1.0, and 2.37, respectively. For all three barrier shapes, the spin injection ratio increases monotonically with the barrier height U but to a varying extent depending on the barrier geometry (see Fig. 4). Barriers with an exponentially decreasing (increasing) slope exhibit the least (greatest) sensitivity to increase in barrier height. Next, we analyze the ef-

fect of barrier geometry (i.e., A_R) on spin injection. As seen from the inset of Fig. 4, there is a substantial decrease in the spin injection ratio with increasing A_R. This is because the effective tunneling resistance of an exponentially decreasing barrier (i.e., with $A_R>1$) is lower than that of an exponentially increasing barrier (with $A_R<1$). This translates to a lower spin injection efficiency, since (as shown in Fig. 3) spin injection generally increases with increasing resistance of the interfacial barrier. While a higher U improves the spin injection ratio γ, the rate of increase in γ is suppressed at large A_R values. It should be noted that barriers with $A_R \approx 2$ have a profile similar to that of a Schottky barrier. Thus, our analysis indicates that a Schottky effect at a FM metal-semiconductor interface is detrimental to achieving high spin injection efficiency, compared to the more squarelike insulating (e.g., oxide) barrier potential of the same tunneling resistance.

In conclusion, we have studied the tunneling spin injection process through an interfacial barrier by means of a self-consistent analysis, which combines the nanoscale Green's function model of tunneling transport within the barrier and the macroscale drift-diffusive model in the contacts. The calculated results show that spin injection efficiency increases with barrier height, as well as barrier asymmetry. The former trend is not obvious and has not been formally predicted previously. Our model also predicts a strong dependence of the spin injection ratio on the barrier profile. In general, an exponentially increasing interfacial barrier between a FM metal and a SC contact yields a higher ratio compared to a Schottky-like exponentially decreasing barrier. This suggests that a pronounced Schottky effect should be avoided in order to achieve a high spin injection ratio. Our calculated results provide a guide to the engineering (e.g., via doping) and biasing of interfacial barriers in order to obtain the optimal barrier height and profile for tunneling spin injection. Finally, beyond the specific study of the influence of barrier profile on spin transport, our self-consistent model also presents several general advantages compared to the purely spin drift-diffusive model. For instance, (a) the barrier resistance, and hence spin injection, is treated as a dynamic quantity, which is coupled to external parameters such as the applied voltage, and (b) microscopic spin transport (e.g., due to local potential variations) and the effects of interactions (electron-electron, electron-phonon, etc.) can be included systematically within the Green's function framework, the latter by inclusion of additional terms to the self-energy apart from that due to the leads, $\Sigma^{L,R}$.

ACKNOWLEDGMENTS

The authors would like to thank the Agency for Science, Technology, and Research (A-STAR) of Singapore, the National University of Singapore (NUS) Grant No. R-263-000-329-112, and Singapore Millennium Foundation (SMF) for financially supporting their work.

[1] S. F. Lee, W. P. Pratt, Jr., R. Loloee, P. A. Schroeder, and J. Bass, Phys. Rev. B **46**, 548 (1992).
[2] S. B. Kumar, S. G. Tan, and M. B. A. Jalil, Appl. Phys. Lett. **90**, 163101 (2007).
[3] M. A. M. Gijs, S. K. J. Lenczowski, and J. B. Giesbers, Phys. Rev. Lett. **70**, 3343 (1993).
[4] G. C. Han, Y. K. Zheng, Z. Y. Liu, B. Liu, and S. N. Mao, J. Appl. Phys. **100**, 063912 (2006).
[5] W. P. Pratt, Jr., S. F. Lee, J. M. Slaughter, R. Loloee, P. A. Schroeder, and J. Bass, Phys. Rev. Lett. **66**, 3060 (1991).
[6] Y. Zheng, Y. Wu, K. Li, J. Qiu, G. Han, Z. Guo, P. Luo, L. An, Z. Liu, L. Wang, S. G. Tan, B. Zong, and B. Liu, J. Nanosci. Nanotechnol. **7**, 117 (2007).
[7] J. S. Moodera, L. R. Kinder, T. M. Wong, and R. Meservey, Phys. Rev. Lett. **74**, 3273 (1995).
[8] J. Schliemann and D. Loss, Phys. Rev. B **68**, 165311 (2003).
[9] S. Datta and B. Das, Appl. Phys. Lett. **56**, 665 (1989).
[10] S. G. Tan, M. B. A. Jalil, and T. Liew, Phys. Rev. B **72**, 205337 (2005).
[11] A. Majumdar, Phys. Rev. B **54**, 11911 (1996).
[12] E. I. Rashba, Phys. Rev. B **62**, R16267 (2000).
[13] A. Fert and H. Jaffres, Phys. Rev. B **64**, 184420 (2001).
[14] H. J. Zhu, M. Ramsteiner, H. Kostial, M. Wassermeier, H. P. Schonherr, and K. H. Ploog, Phys. Rev. Lett. **87**, 016601 (2001).
[15] T. Valet and A. Fert, Phys. Rev. B **48**, 7099 (1993).
[16] S. B. Kumar, M. B. A. Jalil, S. G. Tan, and Z. Y. Leong, Phys. Rev. B **74**, 184426 (2006).
[17] G. Binasch, P. Grunberg, F. Saurenbach, and W. Zinn, Phys. Rev. B **39**, 4828 (1989).
[18] A. Fert and S.-F. Lee, Phys. Rev. B **53**, 6554 (1996).
[19] W. H. Butler, X. G. Zhang, T. C. Schulthess, and J. M. MacLaren, Phys. Rev. B **63**, 054416 (2001).
[20] S. Parkin, C. Kaiser, A. Parnchula, P. M. Rice, B. Hughes, M. Samant, and S.-H. Yang, Nat. Mater. **3**, 862 (2004); S. Yuasa, T. Nagahama, A. Fukushima, Y. Suzuki, and K. Ando, *ibid.* **3**, 868 (2004).
[21] J. D. Albrecht and D. L. Smith, Phys. Rev. B **68**, 035340 (2003).
[22] Jun Wang, H. B. Sun, and D. Y. Xing, Phys. Lett. A **319**, 367 (2003).
[23] V. V. Osipov and A. M. Bratkovsky, Phys. Rev. B **70**, 205312 (2004).
[24] C. Caroli, R. Combescot, P. Nozieres, and D. Saint-James, J. Phys. C **4**, 916 (1971).
[25] J. Mathon, Phys. Rev. B **56**, 11810 (1997).
[26] A. Cresti, R. Farchioni, G. Grosso, and G. P. Parravicini, Phys. Rev. B **68**, 075306 (2003).
[27] S. Nonoyama, A. Oguri, Y. Asano, and S. Maekawa, Phys. Rev. B **50**, 2667 (1994).
[28] R. Lake, G. Klimeck, R. C. Bowen, and D. Jovanovic, J. Appl. Phys. **81**, 7845 (1997).
[29] P. C. van Son, H. van Kempen, and P. Wyder, Phys. Rev. Lett. **58**, 2271 (1987).
[30] D. L. Smith and R. N. Silver, Phys. Rev. B **64**, 045323 (2001).

[31] S. B. Kumar, M. B. A. Jalil, and S. G. Tan, Phys. Rev. B **75**, 155309 (2007).
[32] S. G. Tan, M. B. A. Jalil, S. B. Kumar, G. C. Han, and Y. K. Zheng, J. Appl. Phys. **100**, 063703 (2006).
[33] S. B. Kumar, S. G. Tan, and M. B. A. Jalil, Appl. Phys. Lett. **90**, 142106 (2007).
[34] T. Nozaki, A. Hirohata, N. Tezuka, S. Sugimoto, and K. Inomata, Appl. Phys. Lett. **86**, 082501 (2005).
[35] D.-K. Wang, Q.-F. Sun, and H. Guo, Phys. Rev. B **69**, 205312 (2004).
[36] P. Giannozzi, G. Grosso, S. Moroni, and G. P. Parravicini, Appl. Numer. Math. **4**, 273 (1988).
[37] J. Bass and W. P. Pratt, Jr., J. Magn. Magn. Mater. **200**, 274 (1999).
[38] N. Strelkov, A. Vedyaev, and B. Dieny, J. Appl. Phys. **94**, 3278 (2003).
[39] S. B. Kumar, S. G. Tan, M. B. A. Jalil, and J. Guo, Appl. Phys. Lett. **91**, 142110 (2007).
[40] P. K. Chakraborty and K. P. Ghatak, J. Phys. D **32**, 2438 (1999).